Journal of Solution Chemistry
https://doi.org/10.1007/s10953-024-01405-4

Equilibria Data for the CO_2 + Ethanol + Ketoprofen Systems – Experimental and Modeling

José Vinicius Mattos[1] · Matías José Molina[2,3] · Sabrina Belén Rodriguez-Reartes[2,3,5] · Leandro Ferreira-Pinto[4] · Marcelo Santiago Zabaloy[2,3] · Lúcio Cardozo-Filho[1]

Received: 13 February 2024 / Accepted: 22 July 2024

Abstract

This study investigated the solid–fluid and vapor–liquid equilibrium of varying the molar fraction of ketoprofen in binary system (CO_2 + ketoprofen), 3.14×10^{-5}, 4.70×10^{-5} and 8.11×10^{-5}, and the concentration of ketoprofen in ternary system (CO_2 + ethanol + ketoprofen), 0.05073 and 0.10277 $mol_{Ketoprofen}{\cdot}kg_{ethanol}^{-1}$, on a CO_2-free basis for both systems. The aim was to study the solubility of ketoprofen at different molar fractions and predict its behavior over a wide range of temperatures and pressures by means of thermodynamic modeling. Experiments were conducted as a function of temperature from 313 to 333 K and pressure up to 14 MPa, using a visual synthetic static method with a variable volume cell. The collected data highlight an increase of the ketoprofen solubility with the temperature, while a ketoprofen content has a low impact on the bubble point pressure of the tested ternary system. Data were then correlated by using the thermodynamic modeling employed the Redlich–Kwong–Peng–Robinson equation of state (RK–PR EoS) with quadratic mixing rules for fluid phases and a pure solid model for ketoprofen. Then, a number of complete isopleths at set global composition were computed for the CO_2 + ketoprofen binary system being indicated solid–fluid, solid–fluid–fluid, and fluid–fluid regions. The obtained results suggest that the thermodynamic models used in this work were able to describe the experimentally observed phase behavior.

Graphical Abstract

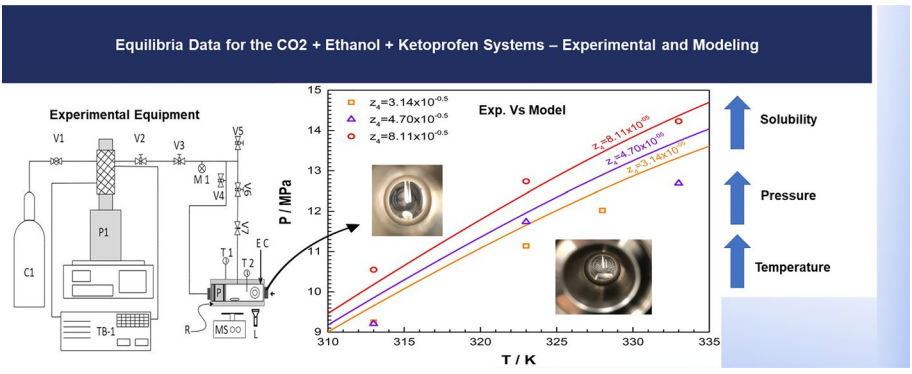

Extended author information available on the last page of the article

Keywords RK-PR EoS · SFE · VLE · Drug · High pressure

Abbreviations

P	Absolute pressure (MPa)
T	Absolute temperature (K)
ω	Acentric factor
k_{ij}	Attractive interaction parameter
$\overline{X}$	Average value of experimental data
C_1, C_2 and C_3	Constants of melting curve of pure compound
$\Delta v^{\mathrm{S-L}}$	Difference of solid and liquid molar volume ($\mathrm{L{\cdot}mol^{-1}}$)
α, β and γ	Double saturation points
ΔH_{fus}	Enthalpy change of fusion ($\mathrm{kJ{\cdot}mol^{-1}}$)
FF	Fluid–Fluid equilibrium
f_i :	Fugacity of component i in the hypothetical liquid state (MPa)
$\widehat{f}_i^{\mathrm{L}}$	Fugacity of compound i in the liquid phase (MPa)
f_i^{S}	Fugacity of pure compound i in solid phase (MPa)
z_4	Global mole fraction of ketoprofen
A	Internal parameters of k_{ij} equation
P	Internal parameters of k_{ij} equation
T_0	Internal parameters of k_{ij} equation (K)
v_{o}	Molar volume ($\mathrm{L{\cdot}mol^{-1}}$)
x_i	Mole fraction of compound i
N	Number of repetitions
P_{tp}	Pressure of triple point (MPa)
l_{ij}	Repulsive interaction parameter
o_i	Solubility of compound i in mole fraction
SFF	Solid–fluid–fluid equilibrium
SF	Solid–fluid equilibrium
$u(X)$	Standard deviation for variable X
T_{fus}	Temperature of fusion (K)
T_{tp}	Temperature of triple point (K)
LV–BP	Transition liquid–vapor in bubble point
X_i	Value of variable X for the $\mathrm{i^{th}}$ experimental data
$k_{ij}^{+\infty}$	Value of the horizontal asymptote of the sigmoid function when T tends to + infinity
$k_{ij}^{-\infty}$	Value of the horizontal asymptote of the sigmoid function when T tends to infinity

1 Introduction

In recent years, significant advances have been made in predicting the aqueous solubility of crystalline drug molecules. From a pharmaceutical standpoint, crystalline solids are frequently preferred when formulating drugs for practical use. Therefore, accurate prediction of the solubility of crystalline drug molecules in different types of solvents would be extremely valuable. This would improve the selection of processes for their production, as well as providing a deeper understanding of how structural modifications affect solubility [1, 2]. Ketoprofen is a nonsteroidal anti-inflammatory drug derived from

2-arylpropionic acid and exhibits efficacy similar to other steroidal anti-inflammatory medications. It is marketed in the racemic form of their R and S enantiomers being widely prescribed for managing conditions such as spondylitis, rheumatoid arthritis, and osteoarthritis, offering antipyretic and analgesic effects. Like sodium naproxen, ketoprofen also acts as a prostaglandin synthesis inhibitor. However, the utilization of this medication has been linked to reported complications, notably gastrointestinal problems, with renal dysfunction and fluid retention being the most frequently observed issues [3]. A crucial challenge with anti-inflammatory drugs lies in their low water solubility, a meager 0.01% by mass. Such limited solubility interferes the drug's bioavailability within human physiology. Several methodologies, such as including surfactants and creating water-soluble salts, have been employed to augment the drug's solubility [4]. The use of supercritical fluids has become increasingly popular in industrial processes [5], replacing traditional methods for a variety of applications such as extraction [6], nanoparticle formation [7], impregnation [8], and polymer synthesis [9].

For these applications, phase equilibrium data are essential for binary and multiphase systems containing carbon dioxide (CO_2), organic solvents, and solids. Information on liquid–liquid, liquid–vapor, and solid–fluid equilibrium is necessary to develop appropriate recrystallization methodologies [10]. CO_2 is a cost-effective and non-toxic compound widely used as a solvent in supercritical extraction due to its high miscibility with other organic solvents used in recrystallization processes [11, 12] and non-flammability. However, solvent selection is critical in processes involving CO_2 because it can act as an antisolvent, leading to precipitation of the solute present in the solution or as a co-solvent, increasing the solubility. This behavior is critical in controlling the solubility and morphology of the solid being purified or recrystallized [1]. Therefore, understanding the behavior of a multiphase system containing solute + organic solvent + CO_2 is crucial for the abovementioned processes. While an extensive body of literature focuses on the empirical determination of solubilities in supercritical fluids [13], a lacuna exists concerning the experimental solubilities of most pharmaceutical compounds in supercritical fluids, especially sc-CO_2. The difficulty of measuring solubility for all possible compounds under a wide range of operational conditions, such as temperature and pressure variations, intensifies this challenge [14, 15].

Consequently, considering these circumstances, predictive tools appear essential for estimating, correlating, and predicting substance solubility in supercritical fluids. The current investigation aims to measure the solubility of ketoprofen using a synthetic method with visual detection of phase transition. In contrast to the literature's experimental data, which utilized a simple static method coupled with a gravimetric method within a wide range of pressure (16.0 to 40.0 MPa) and temperature (308.15 to 338.15 K) [16], the focus of study is evaluating the behavior of solid–fluid and fluid–fluid equilibria in binary {CO_2 + ketoprofen} and ternary {CO_2 + ethanol + ketoprofen} systems at different pressure ranges (7 to 14 MPa). The temperature range considered for the experiments was (313 to 333 K), and the investigation included varying molar fractions and solution concentrations of {ethanol + ketoprofen}. Phase transitions, including bubble points and solid–fluid points, were identified during the study. The thermodynamic model used to describe the non-ideal behavior of the fluid phases was the Redlich–Kwong–Peng–Robinson equation of state (RK–PR EoS) [17] with quadratic mixing rules assuming that the solid phase is composed solely of pure ketoprofen (purity state precipitation), implying a total absence of miscibility in the solid state. The assumption of the total absence of miscibility in the solid state can be reasonable considering the molecular size and shape differences between CO_2 and ketoprofen molecules [18, 19]. Experimental solid–fluid saturation data for various global

compositions were used to fit the parameters of the RK–PR equation of state. Complete isopleths, consisting of solid–fluid and fluid–fluid segments, were calculated for global compositions with available experimental data. Although ketoprofen is widely used as a medicine, limited experimental data are available for producing micro- and nanoparticles in pressurized systems [20]. The main limitations of the equipment are its dependence on the experimentalist's visual ability to observe the phase transition and the very low solubility of the solute. [20]. The proposed study aims to integrate experimental data obtained using the synthetic static variable volume method with thermodynamic modeling of phase behavior using a cubic equation of state. This approach will be applied to construct a phase diagram that covers a wide range of temperatures, pressures, and compositions, thereby enabling the prediction of the drug's behavior in regions not experimentally addressed.

2 Material and Methods

2.1 Materials

The characteristics of the compounds used in the present study are specified in Table 1. It is worth mentioning that the material presented was utilized with no further treatment. The naphthalene used in this study was for verification of the equipment and method, and the ketoprofen is a racemic mixture whose stereoisomeric composition is unknown.

2.2 Method

2.2.1 Differential Scanning Calorimetry (DSC)

The melting temperature (T_{fus}) and enthalpy change of fusion (ΔH_{fus}) were determined using the differential scanning calorimetry (DSC) method. The experimental procedure and equipment were the same as used before by Facchi et al. [21]. The DSC method measures the difference in electrical power of a sample as a function of temperature using a differential calorimeter, which enables precise measurements of the heat of the sample's phase transition. A known amount of the sample was placed in an aluminum dish and heated at a rate of 10 $K \cdot min^{-1}$ under an argon flow of 50 $mL \cdot min^{-1}$, with an operating temperature range of 293 to 573 K. The DSC analysis was performed using a Shimadzu model 60 Plus

Table 1 The characteristics of the compound used in the present work

Compound		Molar Mass $gmol^{-1}$	Chemical formula	CAS number	Supplier	Purity%[a]
(1)	Carbon Dioxide	44.01	CO_2	124–38–9	Linde Gas	> 99.5 (Industrial grade)
(2)	Naphthalene	128.17	$C_{10}H_8$	91–20–3	Sigma Aldrich	> 99.0 wt
(3)	Ethanol	46.07	C_2H_6O	64–17–5	Êxodo Cientifica	> 99.8 wt
(4)	Ketoprofen [b]	254.28	$C_{16}H_{14}O_3$	22,071–15–4	Sigma Aldrich	> 98.0 wt

[a] As stated by the supplier. [b] Racemic mixture

instrument. The instrument was previously calibrated using indium, known for its melting point of 429.78 K, and the calibration result was within the expected range of ± 1.0 K.

2.2.2 Phase Equilibria: Experimental Procedure

The phase equilibrium experiments were conducted using a visual synthetic static method for identifying the phase transition, which involved a variable volume cell operating at high pressures, as illustrated in Fig. 1.

The present phase equilibrium measurement method has been previously introduced in other phase equilibrium studies [5, 22–26]. The experimental setup consisted of a variable volume cell with two sapphire windows for visualizing the cell's interior and illuminating it, a pressure transducer (Smar model M6) with an uncertainty of ± 0.03 MPa, and a syringe pump (ISCO, model 260 D). The cell had a movable internal piston, allowing for internal pressure control. Phase transitions were visually identified by controlling the temperature and reducing the internal pressure of the cell with the syringe pump. Initially, the syringe pump added a pre-weighed amount of the solution (ethanol + ketoprofen) to the cell. The syringe was weighed before and after, on an analytical balance with an uncertainty of ± 0.0001 g, adding the solution to ensure the actual molar fraction. Ketoprofen was solubilized in ethanol at two different molality concentrations for the ternary system, 0.05073 and 0.10277 $mol_{ketoprofen} \cdot kg_{ethanol}^{-1}$, and for the binary system was followed the same procedure but without the solubilization of ketoprofen in ethanol. The system was purged with CO_2 at low pressure to remove residual atmospheric air, and a known amount of CO_2 was fed into the cell using the syringe pump (with a feed uncertainty of 0.005 g). A Teflon-coated magnetic stirrer continuously stirred the cell contents. The temperature was gradually increased to the desired level, with the temperature value having a maximum uncertainty of ± 0.5 K. The pressure was then increased until a single phase was observed in the system. The system was kept under agitation and constant pressure for approximately 30 min to allow for stabilization. The pressure was then slowly reduced (at a rate of 0.1–0.4 $MPa \cdot min^{-1}$) until a new phase was observed. The procedure was repeated at least thrice for the predetermined temperatures and compositions. Standard deviations (u)

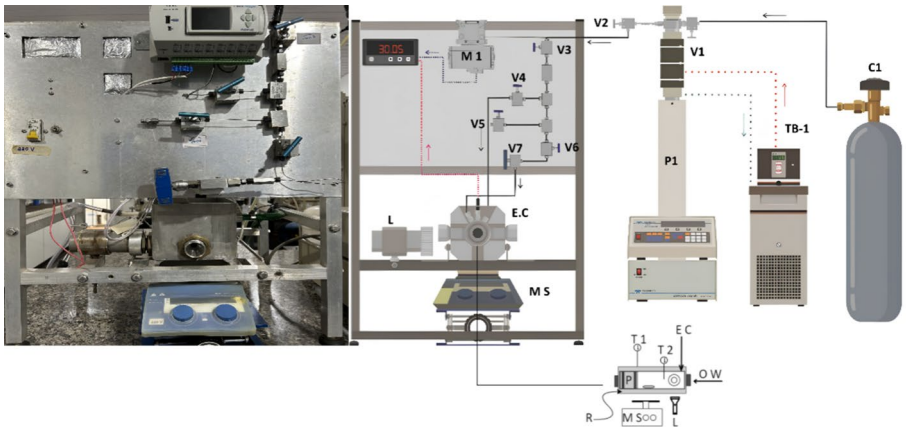

Fig. 1 Phase equilibria apparatus: C1 – CO_2 cylinder, P1 – syringe pump, TB-1 – thermostatic bath, V1 – V6 – valves, V7 – needle valve, M1 – pressure transducer, T1 – T2 – thermocouples, EC – equilibrium cell, O.W – observation window, L – flashlight, R – electric resistance, P – piston and MS – magnetic stirring

were calculated using Eq. 1, where $\bar{x}$ is the mean value, x_i is the observed value, and N is the number of samples.

$$u(X) = \sqrt{\frac{\sum_{i=1}^{N}(X_i - \overline{X})^2}{N-1}} \tag{1}$$

Considering the experimental procedures detailed above, the expanded uncertainty was estimated as described in the literature [27] at 95% of confidence level, and were never greater than 0.11% in mole fraction basis for carbon dioxide, 0.26% in mole fraction basis for naphthalene, were never greater than 7.64×10^{-6} mol fraction of ketoprofen for the binary system and 1.76×10^{-6} for the ternary system, 0.5 K for temperature and 0.1 MPa for pressure.

2.2.3 Modeling of The Phase Behavior of CO_2 (1) + Ketoprofen (4) System

The RK-PR EoS equation has been used to model the phase behavior of the carbon dioxide (1) + ketoprofen (4) system and to compute complete isopleths at set global composition. The interaction parameters of the RK–PR EoS were fitted using the experimental data measured. The primary objective is to determine if the model can accurately replicate the experimental data for SF equilibria with a constant overall composition. Determining a priori whether two components would exhibit partial or complete miscibility in the solid phase is challenging. The extent of solid phase miscibility is deemed insignificant for nonpolar compounds characterized by significant variations in molecular size and shape [28, 29]. Based on practical experience, various empirical guidelines have been employed to forecast the likelihood of solubility in the solid state [30].

Nevertheless, the existing understanding appears inadequate to solely anticipate whether solid solutions or solid precipitation would predominantly occur in a (practically) pure state, or vice versa, without supplementary experimental solid-state data for the system under investigation [30]. The present study has adopted the most straightforward approach, assuming that the solid phase consists solely of pure ketoprofen. In other words, it has assumed a complete lack of miscibility in the solid state, which appears reasonable given the significant molecular size and shape disparities between ketoprofen and CO_2. Furthermore, when considering the two extreme assumptions for the solid state, namely complete miscibility versus complete immiscibility, it is generally more realistic to assume complete immiscibility in most cases [30]. Although this study has chosen to model precipitation in a pure state, there is insufficient evidence to completely dismiss the possibility of CO_2 coexisting with ketoprofen in the solid phase at equilibrium under sufficiently high pressure. The modeling methodology employed in the present study has previously been utilized [31] differing for depicting the phase behavior of binary asymmetric mixtures, where it has assumed that the solid phase consists solely of the pure heavy compound. Similar to the cited references, this study employed the RK–PR–EoS [17] to calculate the fugacity of components in the fluid state for pure compounds and mixtures. For solid–fluid equilibrium calculations, it has been assumed that the solid phase consists solely of pure ketoprofen (4), considering its highly asymmetric mixture with CO_2 (1). "High asymmetry" refers to significant disparities in molecular size and shape between the components in this binary system. The Eq. 2 provides the fugacity of the pure heavy compound in the solid state $f_i^S\left(T,P,v_o\right)$ at the temperature (T) and pressure (P) of the system [31].

$$f_i^S(T,P,v_o) = f_i(T,v_o)\exp(U) \tag{2}$$

In Eq. 2, the symbol v_o corresponds to the molar volume of the pure heavy component (4) when it exists in a (subcooled hypothetical) liquid state at the specific temperature (T) and pressure (P). The fugacity of the pure heavy component in such a pure liquid is $f_i(T,v_o)$. The exponential factor in Eq. 2 establishes the relationship between the hypothetical liquid state and the solid state of a pure substance under specific temperature and pressure conditions. The variable U, which is dependent on temperature (T) and pressure (P), is defined as follows:

$$U = \frac{\Delta v^{S-L}}{RT_{tp}}\left[C_1\left(1-\frac{T_{tp}}{T}\right)+C_2\left(\frac{T_{tp}}{T}-1+\ln\left(\frac{T}{T_{tp}}\right)\right)+C_3\left(\frac{T}{2T_{tp}}-1+\frac{T_{tp}}{2T}\right)+\frac{T_{tp}}{T}(P-P_{tp})\right] \tag{3}$$

within Eq. 3, the constants T_{tp}, P_{tp}, Δv^{S-L}, C_1, C_2, and C_3 are associated with the pure heavy component. Δv^{S-L} is the solid–liquid molar volume difference ($v_{solid} - v_{liquid}$) of the pure component. T_{tp} and P_{tp} represent the triple point temperature and pressure, respectively, of the pure component while R denotes the universal gas constant [31]. The constants C_1, C_2, and C_3, in conjunction with T_{tp} and P_{tp}, define the solid–fluid equilibrium curve (PT melting curve) of the pure heavy component. The system of equations to be solved for computing a phase equilibrium point involving fluid phases and also solid phases each consisting of a pure component arises from imposing the classical necessary equilibrium conditions, which include equal temperatures, equal pressures, and equal fugacity for each component in all phases. In terms of the computational algorithms utilized, we employed numerical continuation methods (NCMs) to compute all phase equilibrium curves [16, 21, 27, 32].

2.2.4 Parameterization of RK-PR—EoS

The interaction parameters k_{ij} and l_{ij} were fitted using experimental solid–fluid saturation data using Eq. 4. The temperature dependence of the attractive parameter k_{ij} implemented in this study is given by the following Eq. 4

$$k_{ij} = k_{ij}^{+\infty} + \frac{A\cdot\left(k_{ij}^{-\infty}-k_{ij}^{+\infty}\right)}{A+\exp\left[p\cdot\left(T-T_0\right)\right]} \tag{4}$$

The Eq. 4 establishes a sigmoidal function of k_{ij} with temperature T. k_{ij} asymptotically tends to $k_{ij}^{+\infty}$ as T approaches positive infinity and to $k_{ij}^{-\infty}$ as T approaches negative infinity (mathematically, since the minimum temperature that could be considered is 0 K). As only three data points are available, and Eq. 4 has five parameters (A, p, T_0, $k_{12}^{+\infty}$ and $k_{12}^{-\infty}$), the values of the horizontal asymptotes $k_{12}^{+\infty}$ and $k_{12}^{-\infty}$ were fixed at − 0.04 and − 0.11, respectively. Then, the remaining three parameters A, p, and T_0 were fitted by the least squares method to the data in Table 2, resulting in the values $A = 22.31$, $p = 9.458\times10^{-2}$, and $T_0 = 288.63$ K. The temperature dependence of the attractive interaction parameter given by Eq. 4 allows k_{ij} to vary only within the temperature range where experimental data exist, remaining nearly constant for very low and very high temperatures where the phase behavior of the binary system CO_2 (1) + ketoprofen (4) is not known.

Table 2 Properties of pure compounds

Compound	T_{tp}/K	P_{tp}/MPa	T_{crit}/K	P_{crit}/MPa	ω
CO_2	216.58[a]	0.521322[b]	304.21[a]	7.38[a]	0.2236[a]
Ketoprofen	366.96[b]	5.31×10^{-9} [b]	882.59[c]	2.5052[c]	1.0091[c]

[a]From DIPPR database [33]. T_{crit}, critical temperature; P_{crit}, critical pressure. ω: acentric factor; [b]Calculated RK–PR–EoS pure compound vapor–liquid equilibrium pressure (P_{tp}) and temperature (T_{tp}) at the triple point (this work); [c]Obtained from group contribution [34]

The properties of the pure substances employed in this study are documented in Table 2. In the RK–PR–EoS, only T_{crit}, P_{crit}, and ω are considered. Due to the lack of data regarding the ketoprofen melting curve, the values of C_2 and C_3 were assumed to be zero. Only the value of C_1 was considered, and it was determined using Eq. 5, and the value is reported in Table 3.

$$C_1 = \frac{\Delta H_{fus}}{\Delta v^{S-L}} \tag{5}$$

3 Results

3.1 Experimental Apparatus Validation

Drug characterization was performed to ensure that the ketoprofen used in present study was the same as the drug used in the literature. Figure 2 shows the DSC analysis data of ketoprofen, which allowed for the calculation of the fusion enthalpy change (ΔH_{fus}) and the

Table 3 Ketoprofen constants for Eq. 3

C_1	− 11,001.20394
C_2	0
C_3	0

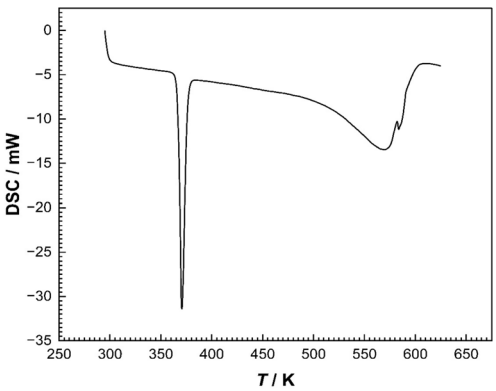

Fig. 2 DSC analysis of ketoprofen

Table 4 Experimental measured and literature data of ketoprofen properties used on phase equilibria

Solid purity%	T_{fus}/K	ΔH_{fus}/kJ·mol^{-1}	References
> 98.0	366.96 ± 0.5	28.5 ± 0.5	This work
–	364.75 ± 2	28.1 ± 1.8	[2]
99.7	366.96 ± 0.02	28.5 ± 0.2	[35]
–	367.36 ± 0.5	28.2 ± 0.3	[36]
> 98.0	367.95 ± 0.12	37.3 ± 0.3	[37]
–	367.19 ± 1.3	21.0 ± 0.8	[38]

T_{fus}—temperature of fusion; ΔH_{fus}—enthalpy change of fusion. Table values for T_{fus} and ΔH_{fus} are followed with standard deviation

melting point (T_{fus}) based on the area under the curve. The experimental results are presented in Table 4 and compared with literature values.

As described in the literature [35], the solubility of ketoprofen varies according to the organic solvent used, and its solubility is also dependent on temperature, the higher the temperature, the greater the solubility of ketoprofen in the organic solvent. The solubility values in molar fraction are shown in Table 5.

The experimental apparatus was validated by comparing the phase equilibrium results of three main systems that have been extensively discussed in the literature, namely {pure CO_2}, {CO_2 (1) + naphthalene (2)}, and {CO_2 (1) + ethanol (3)}.

Table 6 presents the liquid–vapor equilibrium data obtained for CO_2 used in this work with 99.5% of purity, which are compared with data obtained by NIST [39] at three different temperatures: 293 K, 297 K, and 303 K.

The Eq. 6 represents the absolute deviation of calculated pressure and experimental pressure.

Table 5 Literature data of ketoprofen solubility in mole fraction in different solvents [35]

T/K	MeOH	EtOH	*i*-PrOH	BuOH
273.15	0.044 ± 0.001	0.040 ± 0.001	0.0230 ± 0.0007	0.030 ± 0.001
278.15	0.059 ± 0.002	0.056 ± 0.003	0.037 ± 0.001	0.042 ± 0.002
283.15	0.0739 ± 0.0007	0.0634 ± 0.0004	0.044 ± 0.002	0.048 ± 0.002
288.15	0.100 ± 0.004	0.0834 ± 0.0002	0.0618 ± 0.0007	0.0612 ± 0.0005
293.15	0.129 ± 0.001	0.109 ± 0.001	0.0864 ± 0.0001	0.082 ± 0.001
298.15	0.168 ± 0.007	0.1391 ± 0.0003	0.120 ± 0.001	0.111 ± 0.005
303.15	0.192 ± 0.0003	0.1693 ± 0.0006	0.1548 ± 0.0002	0.134 ± 0.004
T/K	ACN	EtAc	Diox	TOL
273.15	0.0096 ± 0.0002	0.045 ± 0.002	0.176 ± 0.002	0.006 ± 0.0003
278.15	0.0121 ± 0.0001	0.050 ± 0.002	0.190 ± 0.005	0.00762 ± 0.00008
283.15	0.0146 ± 0.0002	0.055 ± 0.001	0.204 ± 0.004	0.0107 ± 0.0005
288.15	0.0190 ± 0.0001	0.066 ± 0.001	0.221 ± 0.002	0.0135 ± 0.0002
293.15	0.0249 ± 0.0003	0.080 ± 0.003	0.248 ± 0.004	0.0185 ± 0.0002
298.15	0.03301 ± 0.00009	0.0955 ± 0.0002	0.26 ± 0.01	0.0254 ± 0.0004
303.15	0.0432 ± 0.0004	0.112 ± 0.002	0.275 ± 0.009	0.034 ± 0.001

MeOH, Methanol, EtOH, Ethanol, *i*-PrOH, Isopropanol, BuOH, *n*-Butanol, ACN, Acetonitrile, EtAc, Ethyl acetate, *Diox*, 1,4-Dioxane, TOL, Toluene

Table 6 Results obtained from measuring the liquid–vapor (LV) phase equilibrium of pure CO_2 were compared to those present in NIST

T/K	P/MPa [a]	P/MPa [b]	$\lvert\%\Delta P\rvert$[c]
293.1 ± 0.1	6.04 ± 0.04	5.72	5.30
297.9 ± 0.1	6.73 ± 0.01	6.38	5.20
303.0 ± 0.1	7.34 ± 0.01	7.21	1.77

[a]Pressure of experimental results this work; [b]Ref. [39]; [c]$\lvert\%\Delta P\rvert$ calculated from Eq. 6; Table values for T and P are followed with standard deviation; Standard uncertainties u are $u(T) = 0.5$ K, $u(P) = 0.1$ MPa, never exceed $u(x_{co2}) = 0.11\%$

$$|\%\Delta P| = \frac{\left|P^{\text{calc}} - P^{\text{exp}}\right|}{P^{\text{exp}}} 100 \tag{6}$$

The experimental results shown in Table 6 demonstrate that the accuracy and reliability of the experimental apparatus used are consistent with the literature data, with a difference of pressure not higher than 5.3%.

The equilibrium data of the binary {CO_2 (1) + naphthalene (2)} system obtained experimentally are shown in Figs. 3,4 and compared to literature data [40–48]. Table 7 summarizes the experimental results obtained for this binary system.

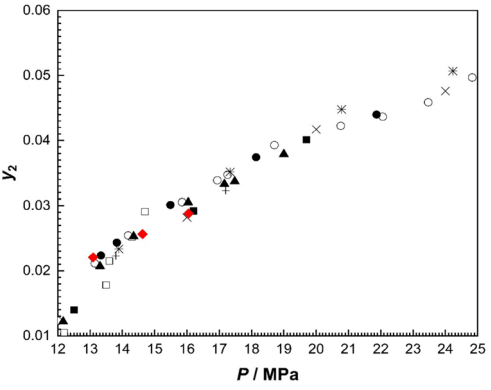

Fig. 3 Solubility of naphthalene (y_2) in CO_2 at 328 K in comparison between data reported in the literature at the same temperature: ◆ – this work; □ – Ref. [43]; Δ – Ref. [48]; ○ – Ref. [45]; ■ – Ref. [44]; +—Ref. [40]; x – Ref. [42]; ⨯ – Ref. [46]; ▲ – Ref. [41]; ● – Ref. [47]

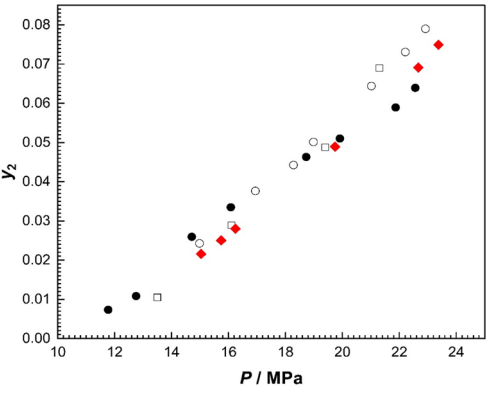

Fig. 4 Solubility of naphthalene (y_2) in CO_2 at 338 K in comparison between data reported in the literature at the same temperature: ◆ – this work; □ – Ref. [43]; ○ – Ref. [45]; ● – Ref. [47]

Table 7 Experimental results obtained from the solubility measuring of the binary system {CO_2 (1) + naphthalene (2)}

y_2	*P*/MPa	y_2	*P*/MPa
T = 328 K		*T* = 338 K	
0.0288	16.05 ± 0.04	0.0749	23.38 ± 0.02
0.0257	14.63 ± 0.04	0.0691	22.67 ± 0.01
0.0221	13.10 ± 0.04	0.0489	19.74 ± 0.01
		0.0288	16.24 ± 0.04
		0.0257	15.74 ± 0.02
		0.0221	15.04 ± 0.05

y_2 – naphthalene solubility in CO_2 (mole fraction); Table values for *P* are followed with standard deviation; Standard uncertainties *u* are $u(T) = 0.5$ K, $u(P) = 0.1$ MPa, never exceed $u(x_{co2}) = 0.11\%$, $u(y_2) = 0.26\%$

Table 8 Experimental results obtained from measuring the liquid–vapor bubble point (LV-BP) phase equilibrium for the binary {CO_2 (1) + ethanol (3)} system

x_{CO2}	*P*/MPa	Transition type
T = 313 K		
0.5074	7.23 ± 0.02	LV-BP
0.5988	7.36 ± 0.01	LV-BP
0.6991	7.82 ± 0.03	LV-BP
0.7995	7.75 ± 0.03	LV-BP
0.8494	7.62 ± 0.02	LV-BP
T = 323 K		
0.5074	8.19 ± 0.09	LV-BP
0.5988	9.07 ± 0.01	LV-BP
0.6991	9.36 ± 0.03	LV-BP
0.7995	9.21 ± 0.03	LV-BP
0.8494	9.22 ± 0.01	LV-BP
T = 333 K		
0.5074	9.30 ± 0.03	LV-BP
0.5988	10.52 ± 0.04	LV-BP
0.6991	10.86 ± 0.02	LV-BP
0.7995	10.75 ± 0.02	LV-BP
0.8494	10.85 ± 0.04	LV-BP

x_{co2} – composition of CO_2 in mole fraction; Table values for *P* are followed with standard deviation; Standard uncertainties *u* are $u(T) = 0.5$ K, $u(P) = 0.1$ MPa, never exceed $u(x_{co2}) = 0.11\%$

The binary {CO_2 (1) + ethanol (3)} system was the third system used to validate the equipment used in the phase equilibrium measurements, and its results are presented in Table 8 and Fig. 5. The experimental data were compared with literature data [49–51].

The validation of the equipment produces phase equilibrium data that are consistent with literature data for the three proposed systems.

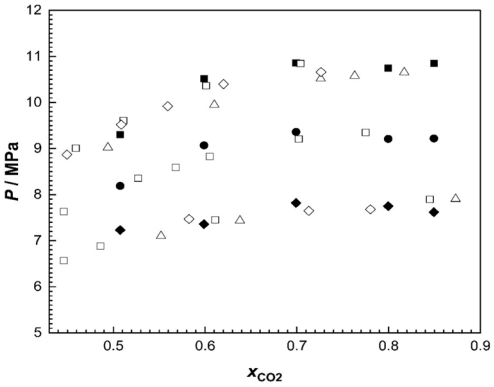

Fig. 5 Experimental vapor – liquid transitions for the {CO_2 (1) + ethanol (3)} system in three different temperatures, 313, 323, and 333 K; ♦ (313 K), ● (323 K) and ■ (333 K) – this work; □ – Ref. [49]; Δ – Ref. [50]; ◊—Ref. [51]

Table 9 Experimental results obtained from measuring the liquid–vapor bubble point (LV-BP) phase equilibrium for the ternary system {CO_2 (1) + ethanol (3) + ketoprofen (4)} at a concentration of 0.05073 $mol_{ketoprofen} \cdot kg_{ethanol}^{-1}$

x_{CO2}	$x_{ketoprofen}$	P / MPa	Transition type
$T = 313$ K			
0.5037	1.16×10^{-3}	7.04 ± 0.01	LV-BP
0.6027	9.26×10^{-4}	7.45 ± 0.02	LV-BP
0.7012	6.97×10^{-4}	7.67 ± 0.02	LV-BP
0.8013	4.63×10^{-4}	7.68 ± 0.02	LV-BP
0.8507	3.48×10^{-4}	7.82 ± 0.02	LV-BP
$T = 323$ K			
0.5037	1.16×10^{-3}	8.13 ± 0.01	LV-BP
0.6027	9.26×10^{-4}	8.78 ± 0.01	LV-BP
0.7012	6.97×10^{-4}	9.18 ± 0.01	LV-BP
0.8013	4.63×10^{-4}	9.21 ± 0.01	LV-BP
0.8507	3.48×10^{-4}	9.37 ± 0.02	LV-BP
$T = 333$ K			
0.5037	1.16×10^{-3}	9.32 ± 0.02	LV-BP
0.6027	9.26×10^{-4}	10.17 ± 0.01	LV-BP
0.7012	6.97×10^{-4}	10.74 ± 0.02	LV-BP
0.8013	4.63×10^{-4}	10.93 ± 0.02	LV-BP
0.8507	3.48×10^{-4}	10.91 ± 0.01	LV-BP

x_{co2} – composition of CO_2 in mole fraction; $x_{ketoprofen}$–composition of ketoprofen in mole fraction; Table values for P are followed with standard deviation; Standard uncertainties u are $u(T) = 0.5$ K, $u(P) = 0.1$ MPa, never exceed $u(x_{co2}) = 0.11\%$, never exceed $u(x_{ketoprofen}) = 1.76 \times 10^{-6}$

3.2 Experimental Data of Binary and Ternary Systems

The phase behavior of both systems is present in Table 9 and Table 11, which contain the experimental data for the binary { CO_2 (1) + ketoprofen (4)} system at molar fraction of 3.14×10^{-5}, 4.70×10^{-5} and 8.11×10^{-5} and ternary { CO_2 (1) + ethanol (3) + ketoprofen (4)} system at concentration of 0.05073 and 0.10277 $mol_{ketoprofen} \cdot kg_{ethanol}^{-1}$ in a CO_2-free basis in the temperature range of 313–333 K. The results shown in Figs. 6, 7 include phase

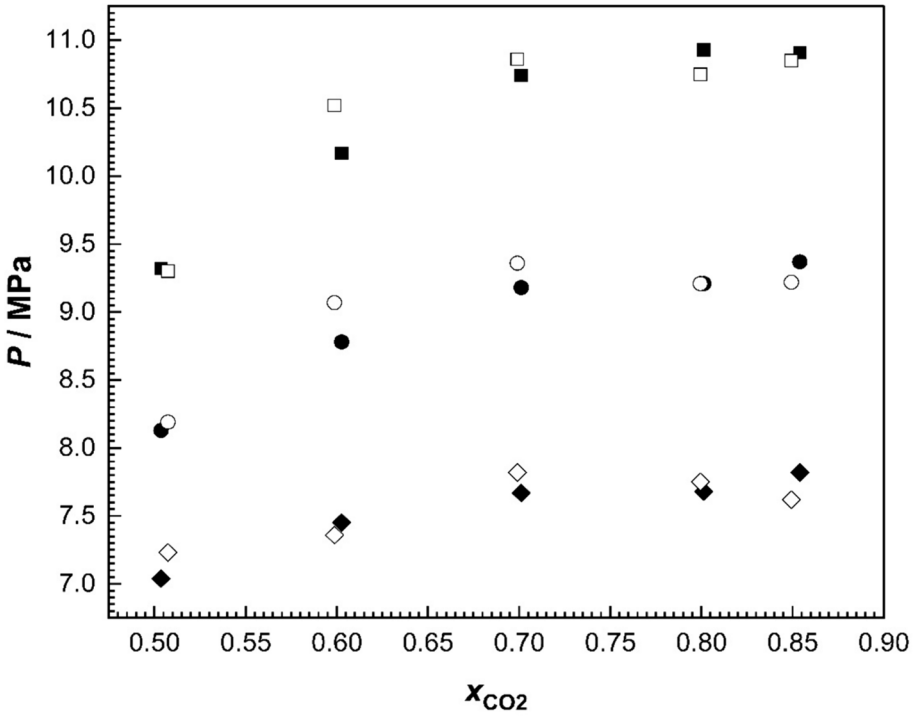

Fig. 6 Experimental vapor–liquid transitions for the system {CO_2 (1) + ethanol (3) + ketoprofen (4)} at 0.05073 mol·kg^{-1} concentration, in comparison with the system {CO_2 (1) + ethanol (3)}, at three different temperatures, 313, 323 and 333 K: ◆ (313 K), ● (323 K) and ■ (333 K) – ternary system; ◇ (313 K), ○ (323 K) and □ (333 K) – binary system

Fig. 7 Experimental vapor–liquid transitions for the system {CO_2 (1) + ethanol (3) + ketoprofen (4)} at 0.10277 mol·kg^{-1} concentration, in comparison with the system {CO_2 (1) + ethanol (3)}, at three different temperature, 313, 323 and 333 K: ◆ (313 K), ■ (323 K) and ● (333 K) – ternary system; ◇ (313 K), ○ (323 K) and □ (333 K) – binary system

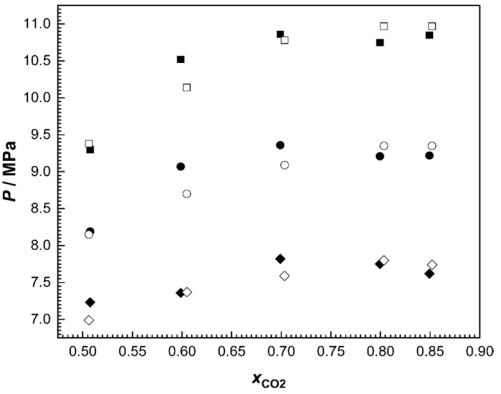

equilibria data for the binary {CO_2 (1) + ethanol (3)} system, allowing for comparison of binary and ternary systems under the same temperature conditions. Table 9 and Table 10 show the experimental results for a two-phase transition of the liquid–vapor type, identified as bubble point (BP). Table 11 presents the comprehensive phase transition data for the binary system consisting of carbon dioxide (1) and ketoprofen (4). Table 11 encompasses

Table 10 Experimental results obtained from measuring the liquid–vapor bubble point (LV-BP) phase equilibrium for the ternary system {CO_2 (1) + ethanol (3) + ketoprofen (4)} at a concentration of 0.10277 $mol_{ketoprofen} \cdot kg_{ethanol}^{-1}$

x_{CO2}	$x_{ketoprofen}$	P/MPa	Transition type
$T = 313$ K			
0.5062	2.32×10^{-3}	6.99 ± 0.02	LV-BP
0.6049	1.86×10^{-3}	7.37 ± 0.01	LV-BP
0.7034	1.40×10^{-3}	7.59 ± 0.01	LV-BP
0.8036	9.26×10^{-4}	7.80 ± 0.02	LV-BP
0.8520	6.97×10^{-4}	7.74 ± 0.02	LV-BP
$T = 323$ K			
0.5062	2.32×10^{-3}	8.15 ± 0.03	LV-BP
0.6049	1.86×10^{-3}	8.70 ± 0.01	LV-BP
0.7034	1.40×10^{-3}	9.09 ± 0.02	LV-BP
0.8036	9.26×10^{-4}	9.35 ± 0.01	LV-BP
0.8520	6.97×10^{-4}	9.35 ± 0.01	LV-BP
$T = 333$ K			
0.5062	2.32×10^{-3}	9.38 ± 0.02	LV-BP
0.6049	1.86×10^{-3}	10.14 ± 0.01	LV-BP
0.7034	1.40×10^{-3}	10.78 ± 0.03	LV-BP
0.8036	9.26×10^{-4}	10.97 ± 0.01	LV-BP
0.8520	6.97×10^{-4}	10.97 ± 0.01	LV-BP

x_{co2} – composition of CO_2 in mole fraction; $x_{ketoprofen}$ – composition of ketoprofen in mole fraction; Table values for P are followed with standard deviation; Standard uncertainties u are $u(T) = 0.5$ K, $u(P) = 0.1$ MPa, never exceed $u(x_{co2}) = 0.11\%$, never exceed $u(x_{ketoprofen}) = 1.76 \times 10^{-6}$

Table 11 Experimental results obtained from measuring the solid–fluid (SF) transition for the binary system {CO_2 (1) + ketoprofen (4)} with ketoprofen in insipient solid phase

$x_{ketoprofen}$	P/MPa	P_{calc}/MPa[a]	$\lvert\%\Delta P\rvert$[b]	Transition type
$T = 313$ K				
3.14×10^{-5}	9.25 ± 0.03	9.65	4.19	SF
4.70×10^{-5}	9.21 ± 0.05	9.85	6.55	SF
8.11×10^{-5}	10.55 ± 0.03	10.18	3.60	SF
$T = 323$ K				
3.14×10^{-5}	11.14 ± 0.05	11.65	4.42	SF
4.70×10^{-5}	11.74 ± 0.02	11.96	1.85	SF
8.11×10^{-5}	12.74 ± 0.06	12.44	2.38	
$T = 328$ K				
3.14×10^{-5}	12.02 ± 0.04	12.54	4.16	SF
$T = 333$ K				
4.70×10^{-5}	12.69 ± 0.06	13.73	7.63	SF
8.11×10^{-5}	14.23 ± 0.06	14.37	0.98	SF

$x_{ketoprofen}$ – composition of ketoprofen in mole fraction; [a] calculated pressure by the thermodynamic model RK-PR EoS; [b] $\lvert\%\Delta P\rvert$ calculated from Eq. 6; Table values for P are followed with standard deviation; SF – solid–fluid transition with insipient solid phase; Standard uncertainties u are $u(T) = 0.5$ K, $u(P) = 0.1$ MPa, never exceed $u(x_{co2}) = 0.11\%$, never exceed $u(x_{ketoprofen}) = 7.64 \times 10^{-6}$

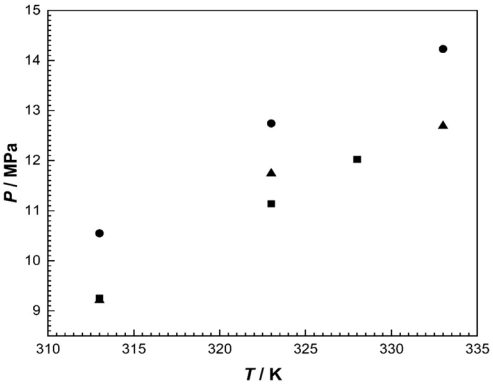

Fig. 8 Experimental solid – Fluid transitions for the binary {CO_2 (1) + ketoprofen (4)}. The system consists of three concentrations of ketoprofen (3.14×10^{-5}, $4.70\times10^{-5}$and 8.11×10^{-5}) at temperatures of 313 K, 323 K, 328 K, and 333 K, respectively: ■ (concentration of 3.14×10^{-55} at 313, 323 and 328 K), ▲ (concentration of 4.70×10^{-5} at 313, 323 and 333 K) and ● (concentration of 8.11×10^{-5} at 313, 323 and 333 K)

the solid–fluid system and a temperature range from 313 to 333 K. The corresponding experimental findings are visually depicted in Fig. 8.

Table 11 shows the experimental data for composition, temperature, phase transition pressure (P), and the pressure values calculated (P_{calc}) by the RK-PR model. In Table 11, the results of the absolute deviation are less than 10%, it represents an acceptable result of the thermodynamic model and the experimental data. No formation of precipitate or suspended solids was observed in the measured phase transition data for the ternary system {CO_2 (1) + ethanol (3) + ketoprofen (4)}. In the binary system {CO_2 (1) + ketoprofen (4)}, the solid formation of ketoprofen is directly influenced by the temperature of the system and the density of sc-CO_2. This behavior is explained in the literature as due to the association of vapor pressure, which increases with temperature [16]. According to the literature [16] as the system's pressure rises, the density of CO_2 also increases, which in turn leads to a higher solvating strength, the same behavior is observed in the experimental data of this work.

Figure 8 shows the P–T diagram of the experimental data for the binary system {CO_2 (1) + ketoprofen (4)} contained in Table 11.

Figures 9 (a), 9 (b) and 9 (c) compare the experimental solid–fluid phase transition data measured in this work and those reported in the literature [14–16, 52] for the binary system CO_2 (1) + ketoprofen (4). The experimental solubility data reported in the literature for the binary system CO_2 (1) + ketoprofen (4) employed the dynamic analytical method and its variations. In addition, the purity of the CO_2 used in the solubility measurements of ketoprofen in CO_2 reported in the literature is between 99.98 and 99.999% by volume. The purity of the CO_2 used in this study was 99.5% (industrial grade). The industrial grade of CO_2 used in this work and the dynamic analytical method, and its variations used to measure ketoprofen solubility in CO_2 reported in the literature reflect the differences observed between the solubility data of the CO_2 (1) + ketoprofen (4) binary system measured and those reported in the literature.

For the Fig. 9, the solubility of ketoprofen in a solvent-free base was expressed using Eq. 2 given in the literature [53], where the mole fraction of the solute is divided by the sum of the mole fractions of the solvents, or analogously, 1 – xs, where xs is the mole fraction of the solute. As in Ref. [53], this solute solubility is indicated by y_4, as shown in Eq. 7.

$$y_4 = \frac{xs}{1 - xs} \tag{7}$$

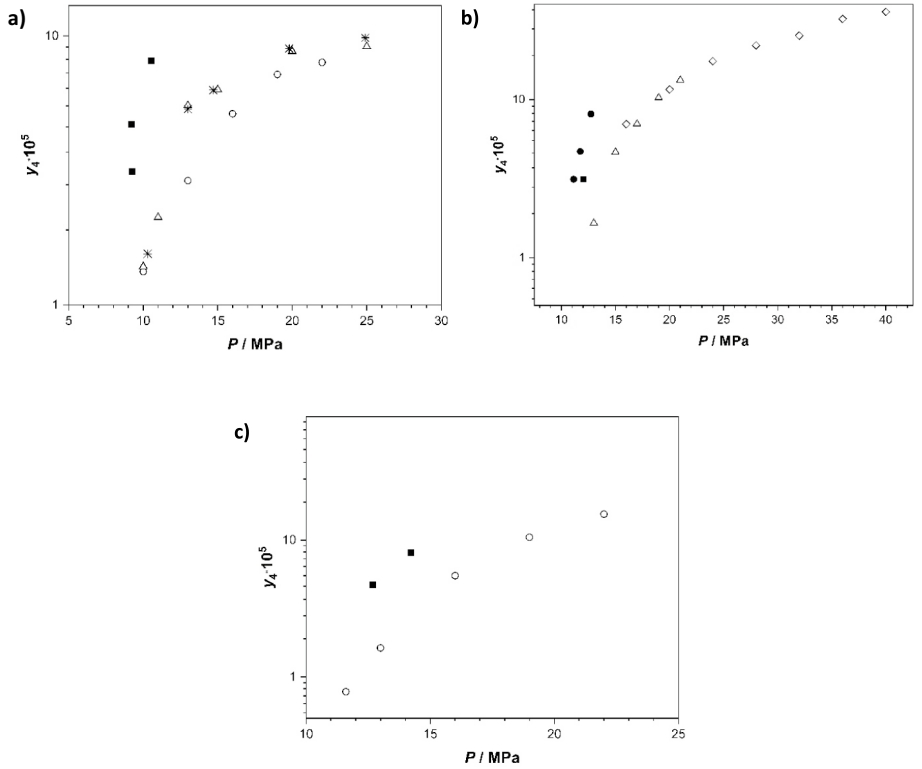

Fig. 9 Solubility of ketoprofen in sc-CO_2 as a function of pressure P compared to data reported in the literature; **a)** ■ – this work (313 K), Δ – Ref. [14] (313 K), ○ – Ref [15]. (313 K), and ⁎—Ref. [52] (313 K); **b)** ■ – this work (323 K), ● – this work (328 K), Δ – Ref. [14] (328 K) and ◇—Ref. [16] (328 K); **c)** ■ – this work (333 K), ○ – Ref. [15] (333 K)

3.3 Modeling Results

The temperature-dependent attractive interaction parameter and the repulsive interaction parameter of the RK-PR EoS for fluid phases were fitted in this work to experimental carbon dioxide (1) + ketoprofen (4) solid–fluid equilibrium data due to the lack of experimental fluid–fluid equilibrium data. The value of the repulsive parameter l_{ij} was adjusted to ensure an appropriate relative stability continuity between the calculated fluid–fluid and solid–fluid saturation curves. The k_{ij} interaction parameter was calculated for each experimental point in Table 12 by solving the Eq. 8 derived from the imposition of the isofugacity condition for ketoprofen at the specified temperature and pressure for solid–fluid equilibrium. The fugacity of component "i" $\hat{f}_i^{\mathrm{L}}(T, z, v_L)$ in the liquid phase is dependent of T, v_{L} and the vector of global composition **z**.

$$\widehat{f}_i^{\mathrm{L}}\left(T, \mathbf{z}, v_{\mathrm{L}}\right) = f_i^{\mathrm{S}}(T, P, v_{\mathrm{HL}}) \tag{8}$$

Experimental data points 2 and 9, corresponding to $z_4 = 4.70 \times 10^{-5}$, were not considered in the fit due to the non-monotonic isoplectic behavior, unlike the sets of experimental data points corresponding to $z_4 = 3.14 \times 10^{-5}$ and $z_4 = 8.11 \times 10^{-5}$. Furthermore, experimental

Table 12 Experimental data for solid–fluid saturation points for the CO_2 (1) + ketoprofen (4) system, and interaction parameters k_{ij} calculated for $l_{ij} = -0.05$

Points number	*T*/K	*P*/MPa	Global mole fraction of ketoprofen z_4	$k_{ij,\,calc}$
1	313	9.25	3.14×10^{-5}	− 0.1197
2	313	9.21	4.70×10^{-5}	not included
3	313	10.55	8.11×10^{-5}	− 0.05691
4	323	11.14	3.14×10^{-5}	− 0.09536
5	323	11.77	4.70×10^{-5}	− 0.07030
6	323	12.74	8.11×10^{-5}	− 0.04661
7	328	12.02	3.14×10^{-5}	not included
8[a]	333	12.86	3.14×10^{-5}	− 0.06902
9	333	12.69	4.70×10^{-5}	not included
10	333	14.23	8.11×10^{-5}	− 0.04768

[a] Pseudo-experimental point created for fitting purposes

data point 7 in Table 12, corresponding to $z_4 = 3.14 \times 10^{-5}$, was excluded from the adjustment because it is the only one measured at a temperature of 328 K. The k_{ij} values calculated for the same temperature were averaged, resulting in a single k_{ij} value for each temperature, regardless of the global composition of the system, as shown in Table 13.

Figure 10 illustrates how the attractive parameter k_{ij} varies with the temperature for the CO_2 (1) + ketoprofen (4) binary system present in this work.

The thermodynamic modeling approach described, and the parameters provided in Table 2, Table 3, and Table 12, Table 13 were used to represent the measured experimental data of the CO_2 (1) + ketoprofen (4) system. Part of the isopleths corresponding to the measured experimental global compositions was also generated.

Table 13 Interaction parameters calculated for the CO_2 (1) + ketoprofen (4) system for $l_{ij} = -0.05$

T/K	$k_{ij,\,average}$
313	− 0.08830
323	− 0.07076
333	− 0.05835

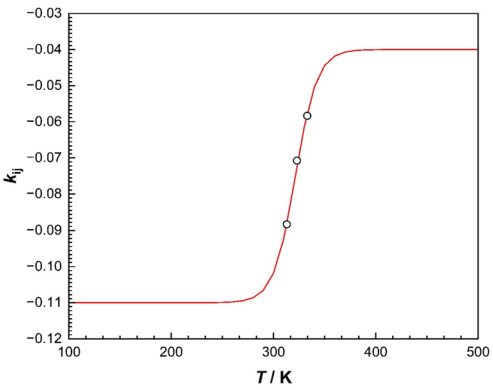

Fig. 10 Behavior of the interaction parameter k_{ij} as a function of temperature for the CO_2 (1) + ketoprofen (4) system according to Eq. 4. ○—Calculated values of k_{ij} shown in Table 13

Figure 11a shows the pressure versus temperature projection of the calculated isopleth for the system CO_2 (1) + ketoprofen (4) for the global mole fraction $z_4 = 3.14 \times 10^{-5}$. The isopleth of Fig. 11a is composed of two solid–fluid (SF) segments, two fluid–fluid (FF) segments, calculated following the methodology as proposed in the literature [19, 30], respectively, and two segments of three-phase curves (SFF) compatible with the global composition, calculated by a methodology similar to that used in the literature [18]. Three experimental SF data points obtained for the global composition $z_4 = 3.14 \times 10^{-5}$ are included in Fig. 11a (indicated with □). The points indicated as α, β, and γ in Fig. 11a are double saturation points compatible with the specified global composition. At points α and β, there is an equilibrium between a major liquid phase with the global mole fraction $z_4 = 3.14 \times 10^{-5}$, a fluid phase, and an incipient solid phase formed by pure ketoprofen. At the double saturation point γ, a major vapor phase with a global mole fraction of $z_4 = 3.14 \times 10^{-5}$ coexists in equilibrium with an incipient liquid phase and with an incipient solid phase formed by pure ketoprofen.

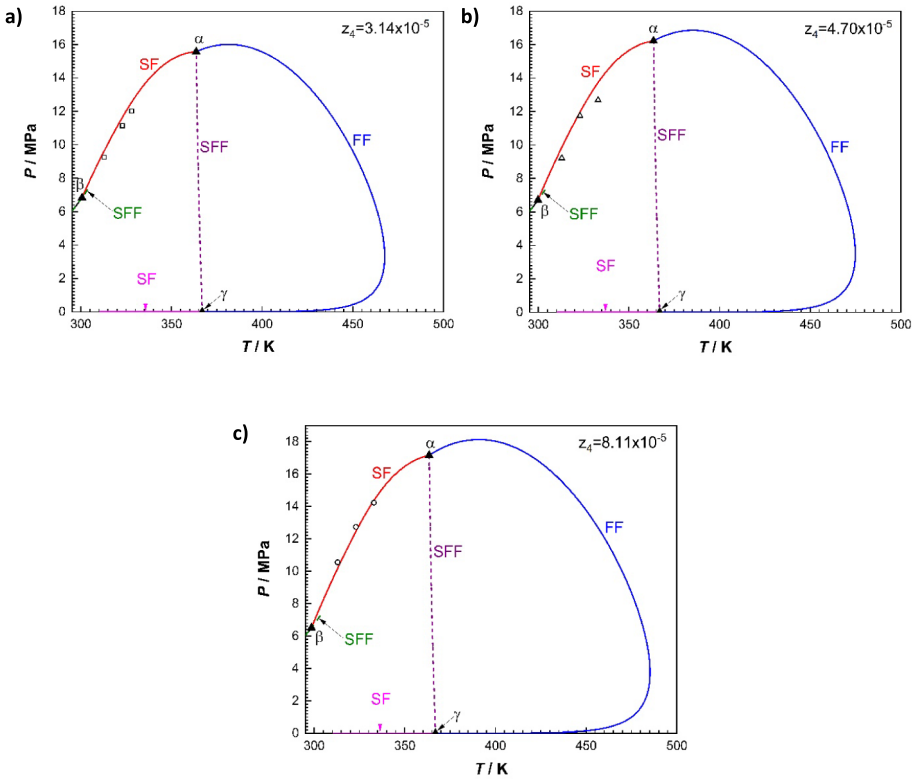

Fig. 11 Pressure—temperature projection of the Isopleths calculated for the CO_2 (1) + ketoprofen (4) system with: **a)**: $z_4 = 3.14 \times 10^{-5}$. □—Experimental data; **b)** $z_4 = 4.70 \times 10^{-5}$. △—Experimental data; **c)** $z_4 = 8.11 \times 10^{-5}$. ○—Experimental data. ▲: solid–fluid-fluid double saturation points. Red SF curve: Solid–fluid saturation curve (incipient solid). Black FF curve: Fluid–fluid saturation curve. Magenta SF curve: Solid–vapor saturation curve (incipient solid). Blue FF curve: Fluid–fluid saturation curve. Dashed violet SFF curve and dashed green SFF curve: Segments of solid–fluid-fluid three-phase curves compatible with the value of z_4. Model: RK–PR EoS with quadratic mixing rules, k_{ij} from Fig. 10, and $l_{ij} = -0.05$

The red SF curve is a solid–fluid saturation curve. At each point of the red SF curve a major liquid phase (L) is at equilibrium with an incipient solid phase formed by pure ketoprofen. The red SF curve starts at point α and extends at low temperatures and low pressures until it ends at point β. The metastable segments of the red SF curve are not shown in Fig. 11a. The blue FF curve is a fluid–fluid saturation curve that starts at the γ point at low temperatures and low pressures like a dew point curve and ends at the α point at high temperatures and high pressures as a cloud point curve. Along the blue FF curve, there is no FF-type critical point. The continuous magenta SF curve is a solid–fluid saturation curve where a major vapor phase with global mole fraction $z_4 = 3.14 \times 10^{-5}$ coexists at equilibrium with an incipient solid phase formed by pure ketoprofen. The magenta SF curve starts at the γ double saturation point and extends indefinitely for low temperatures and low pressures.

The complete isopleths, derived from the thermodynamic model and experimental data of the {CO_2 + ketoprofen} system, are depicted in Fig. 11a, b, c. Analysis of these curves reveals that elevated temperatures increase transition pressure and alterations in the type of transition observed. Initially, there is a shift from a solid–fluid–fluid (SFF) equilibrium, passing through a β double saturation point, to a solid–fluid (SF) equilibrium in the region of the experimental data and subsequently to a fluid–fluid (FF) equilibrium after the α double saturation point. The transition pressure for the FF equilibrium continues to rise until approximately 400 K (maximum pressure); beyond this point, the pressure begins to decrease with further temperature increases. This trend is consistent across the three studied concentrations. With a decrease in temperature following the maximum temperature, the transition pressure declines, reaching a new γ double saturation point and reversing the equilibrium from FF to SF. This behavior is consistent across all isopleths. A purple dashed line connects the points of double saturation α and γ, demarcating the SFF equilibrium region and delimiting the solid phase region.

The dashed violet curve shown in Fig. 11a is a segment of a three-phase curve compatible with the specified global mole fraction $z_4 = 3.14 \times 10^{-5}$ (segments of the SFF curve that are not compatible with $z_4 = 3.14 \times 10^{-5}$ are not shown in Fig. 11. It extends from the double saturation point α and ends at the double saturation point γ. On the other hand, the dashed green SFF curve is a segment of a solid–fluid–fluid three-phase curve compatible with $z_4 = 3.14 \times 10^{-5}$. It extends from a critical end point (not indicated in Fig. 11) at a temperature of approximately 304 K toward low temperatures and low pressures, passing through the double saturation point β. When computing this line, it was found to self-intersect, presenting metastable three-phase segments. This indicates a solid–fluid–fluid quadruple point at approximately 295 K and 6.03 MPa. This quadruple point is not shown in Fig. 11a.

Finally, the black FF curve is a fluid–fluid saturation curve that originates at point β and extends toward low temperatures and low pressures. This FF saturation curve is above the dashed green SFF curve; however, due to the temperature and pressure scale used, both curves may be superimposed in the pressure vs temperature plane. The red SF curve calculated for $z_4 = 3.14 \times 10^{-5}$ is consistent with the experimental data obtained for the same global composition, meaning that the model is capable of describing, at least qualitatively, the observed experimental behavior for the CO_2 (1) + ketoprofen (4) system at $z_4 = 3.14 \times 10^{-5}$.

Figures 11b, c show the pressure versus temperature projections of the isopleths computed for $z_4 = 4.70 \times 10^{-5}$ and $z_4 = 8.11 \times 10^{-5}$, respectively, along with the experimental data obtained for the same global compositions. These isopleths are analogous to the one

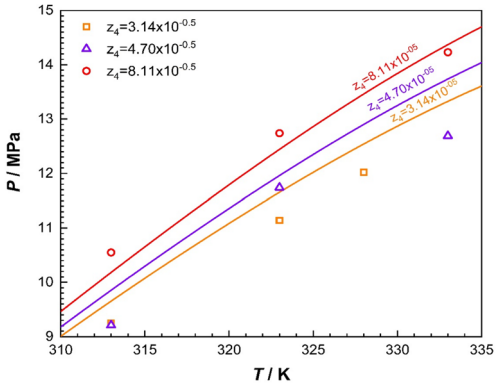

Fig. 12 Pressure—temperature projection of the SF saturation segment of the isopleths calculated for the CO_2 (1) + ketoprofen (4) system. Δ represents the experimental data of the mole fraction of ketoprofen value (3.14×10^{-5}); □ represents the experimental data of the mole fraction of ketoprofen value (4.70×10^{-5}), and ○ represents the experimental data of the mole fraction of ketoprofen value (8.11×10^{-5}). The continuous line is for the first isopleth, the semi-continuous is for the second isopleth, and the dot line is for the third isopleth

corresponding to the global mole fraction $z_4 = 3.14\times10^{-5}$ shown in Fig. 11a; therefore, the phase behavior analysis is the same.

The isopleths shown in Fig. 12 represent the modeling based on the experimental data of the binary system at the respective ketoprofen mole fractions of 3.14×10^{-5}, 4.70×10^{-5} and 8.11×10^{-5}. It can be observed in Fig. 12 that the slope of the SF saturation lines of the isopleths are positive, just like those of the experimental points for each global composition. Furthermore, as the global molar fraction of ketoprofen increases, the SF saturation curve shifts toward higher pressures and the size of the SF heterogeneous region increases.

In the Fig. 8 and Fig. 12, the saturation points of the solid and liquid should increase monotonically between 313 and 333 K for each composition. However, in the Table 12, the points 2 and 9 ($z_4 = 4.70\times10^{-5}$) do not align with point 5 and are below a trend line that should pass through points 1, 4, and 7. This behavior is unexpected because, as the overall mole fraction of component 4 increases, the saturation points of the solid and liquid should shift toward higher pressures, all else being equal. The discrepancy between points 2 and 9 may be associated with experimental uncertainties or perhaps other factors we have not yet identified.

4 Conclusion

This study investigated the phase transitions of systems {CO_2 (1) + ketoprofen (4)} and {CO_2 (1) + ethanol (3) + ketoprofen (4)} at temperatures of (313–333) K and pressures up to 14 MPa. Experimentally, it observed the solid–fluid phase transition at a binary system containing CO_2 and ketoprofen, and phase transition vapor–liquid was observed at a ternary system composed of CO_2, ethanol, and ketoprofen. Results also revealed that in a binary system, the temperature and pressure are significant factors for the ketoprofen solubility, implying the solid formation and this approach facilitate the understanding of the system's behavior in precipitation or recrystallization processes involving CO_2. In the ternary system, with the presence of ethanol, solid precipitation was not observed in any range of experimental temperatures. Furthermore, the drug at low concentrations has

shown no significant influence in the phase equilibria between the binary system involving CO_2 and ethanol and the ternary system. The thermodynamic modeling results showed a vast region of solid–fluid equilibrium in different temperature and pressure ranges. This approach allows an understanding of the binary system's behavior and identifies the drug's precipitation regions in carbon dioxide. These results help produce microparticles or recrystallization processes in which sc-CO_2 acts as an antisolvent. Additionally, DSC thermal analyses were performed to ensure that the drug used had the same characteristics reported in the literature.

Supplementary Information The online version contains supplementary material available at https://doi.org/10.1007/s10953-024-01405-4.

Acknowledgements This work has received financial support with Scholarships from the Brazilian National Council of Technological and Scientific Development, CNPq and the Coordination for the Improvement of Higher Education Personnel, CAPES.

Author Contribution We, the undersigned, declare that this manuscript is original, has not been published before, and is not currently being considered for publication elsewhere. We confirm that the manuscript has been read and approved by all named authors and that there are no other persons who satisfied the criteria for authorship but are not listed. We further confirm that all have approved the order of authors listed in the manuscript. We understand that the Corresponding Author is the sole contact for the Editorial process. He is responsible for communicating with the other authors about progress, submissions of revisions, and final approval of proofs. So, on behalf of all authors, it is signed as follows. Yours sincerely, Lucio Cardozo Filho Universidade Estadual de Maringá—UEM Postgraduation Program in Chemical Engineering Maringá – Paraná – Brazil CEP—87,020,900 lcfilho@uem.br.

Data Availability No datasets were generated or analyzed during the current study.

Declarations

Competing Interest The authors declare no competing interests.

References

1. Lazzaroni, M.J., Bush, D., Brown, J.S., Eckert, C.A.: High-pressure vapor-liquid equilbria of some carbon dioxide + organic binary systems. J. Chem. Eng. Data **50**, 60–65 (2005)
2. Mura, P., Bettinetti, G.P., Manderioli, A., Faucci, M.T., Bramanti, G., Sorrenti, M.: Interactions of ketoprofen and ibuprofen with i-cyclodextrins in solution and in the solid state. Int. J. Pharm. **166**, 189–203 (1998)
3. Jamali, F., Brocks, D.R.: Clinical pharmacokinetics of ketoprofen and its enantiomers. Clin. Pharmacokinet. **19**, 197–217 (1990)
4. Yiyun, C., Tongwen, X., Rongqiang, F.: Polyamidoamine dendrimers used as solubility enhancers of ketoprofen. Eur. J. Med. Chem. **40**, 1390–1393 (2005)
5. Giufrida, W.M., Pinto, L.F., Zanette, A.F., Voll, F.A.P., Kunita, M.H., Cabral, V.F., Cardozo-Filho, L.: Liquid–vapor equilibrium data of CO_2 + dichloromethane + medroxyprogesterone system. Fluid Phase Equilib. **362**, 307–312 (2014)
6. Sodeifian, G., Sajadian, S.A.: Investigation of essential oil extraction and antioxidant activity of Echinophora Platyloba DC. using supercritical carbon dioxide. J. Supercrit. Fluids **121**, 52–62 (2017)
7. Sodeifian, G., Sajadian, S.A.: Solubility measurement and preparation of nanoparticles of an anticancer drug (Letrozole) using rapid expansion of supercritical solutions with solid cosolvent (RESS-SC). J. Supercrit. Fluids **133**, 239–252 (2018)
8. Ameri, A., Sodeifian, G., Sajadian, S.A.: Lansoprazole loading of polymers by supercritical carbon dioxide impregnation: impacts of process parameters. J. Supercrit. Fluids **164**, 104892 (2020)
9. Daneshyan, S., Sodeifian, G.: Synthesis of cyclic polystyrene in supercritical carbon dioxide green solvent. J. Supercrit. Fluids **188**, 105679 (2022)

10. Stievano, M., Elvassore, N.: High-pressure density and vapor–liquid equilibrium for the binary systems carbon dioxide–ethanol, carbon dioxide–acetone and carbon dioxide–dichloromethane. J. Supercrit. Fluids **33**, 7–14 (2005)
11. Subramaniam, B., Rajewski, R.A., Snavely, K.: Pharmaceutical processing with supercritical carbon dioxide. J. Pharm. Sci. **86**, 885–890 (1997)
12. Kikic, I., De Zordi, N., Moneghini, M., Solinas, D.: Solubility estimation of drugs in ternary systems of interest for the antisolvent precipitation processes. J. Supercrit. Fluids **55**, 616–622 (2010)
13. Dohrn, R., Fonseca, J.M.S., Peper, S.: Experimental methods for phase equilibria at high pressures. Annu. Rev. Chem. Biomol. Eng. **3**, 343–367 (2012)
14. Stassi, A., Bettini, R., Gazzaniga, A., Giordano, F., Schiraldi, A.: Assessment of solubility of ketoprofen and vanillic acid in supercritical CO_2 under dynamic conditions. J. Chem. Eng. Data **45**, 161–165 (2000)
15. Macnaughton, S.J., Kikic, I., Foster, N.R., Alessi, P., Cortesi, A., Colombo, I.: Solubility of anti-inflammatory drugs in supercritical carbon dioxide. J. Chem. Eng. Data **41**, 1083–1086 (1996)
16. Sabegh, M.A., Rajaei, H., Esmaeilzadeh, F., Lashkarbolooki, M.: Solubility of ketoprofen in supercritical carbon dioxide. J. Supercrit. Fluids **72**, 191–197 (2012)
17. Cismondi, M., Mollerup, J.: Development and application of a three-parameter RK–PR equation of state. Fluid Phase Equilib. **232**, 74–89 (2005)
18. Rodriguez-Reartes, S.B., Cismondi, M., Zabaloy, M.S.: Computation of Solid–Fluid–Fluid equilibria for binary asymmetric mixtures in wide ranges of conditions. J. Supercrit. Fluid **57**, 9–24 (2011)
19. Rodriguez-Reartes, S.B., Guapacha, J.A., Zabaloy, M.S.: Characterization of solid-fluid equilibrium regions of computed constant-overall-composition phase diagrams. J. Supercrit. Fluids **130**, 210–229 (2017)
20. Peper, S., Fonseca, J.M.S., Dohrn, R.: High-pressure fluid-phase equilibria: trends, recent developments, and systems investigated (2009–2012). Fluid Phase Equilib. **484**, 126–224 (2019)
21. Facchi, D.P., Cazetta, A.L., Canesin, E.A., Almeida, V.C., Bonafé, E.G., Kipper, M.J., Martins, A.F.: New magnetic chitosan/alginate/Fe_3O_4@Sio_2 hydrogel composites applied for removal of Pb(II) ions from aqueous systems. Chem. Eng. J. **337**, 595–608 (2018)
22. Giufrida, W.M., Rodriguez-Reartes, S.B., Alonso, C.G., Zabaloy, M.S., Cabral, V.F., Tavares, F.W., Cardozo-Filho, L.: High-pressure experimental data of CO_2 + mitotane and CO_2 + ethanol + mitotane mixtures. J. Chem. Eng. Data **56**, 4333–4341 (2011)
23. Favareto, R., Fregadolli, P.H., Cabral, V.F., Antunes, O.A.C., Cardozo-Filho, L.: Phase equilibria of acrylonitrile and *p*-bromobenzaldehyde in carbon dioxide. J. Chem. Eng. Data **53**, 1080–1084 (2008)
24. Dos Santos, J.C., Mazzer, H.R., Machado, G.D., Andreaus, J., Cabral, V.F., Zabaloy, M.S., Cardozo-Filho, L.: High-pressure phase behaviour of the system (CO_2 + C.I. disperse orange 30 dye). J. Chem. Thermodyn. **48**, 284–290 (2012)
25. Pinto, L.F., Ndiaye, P.M., Ramos, L.P., Corazza, M.L.: Phase equilibrium data of the system CO_2 + glycerol + methanol at high pressures. J. Supercrit. Fluids **59**, 1–7 (2011)
26. Bacicheti, J.M.O., Oliveira, J.A., Barros, T.V., Ferreira-Pinto, L., Castillo, P.F.A., Cabral, V.F., Cardozo-Filho, L.: Phase equilibria of carbon dioxide + acetone + dimethyl sulfoxide systems: experimental data and thermodynamic modeling. J. Solution Chem. **51**, 1292–1309 (2022)
27. Rodriguez-Reartes, S.B., Cismondi, M., Franceschi, E., Corazza, M.L., Oliveira, J.V., Zabaloy, M.S.: High-pressure phase equilibria of systems carbon dioxide + *n*-eicosane and propane + *n*-eicosane. J. Supercrit. Fluids **50**, 193–202 (2009)
28. Prausnitz, J.M., Lichtenthaler, R.N., De Azevedo, G.: Molecular Thermodynamics of Fluid-Phase Equilibria. Prentice-Hall PTR, New Jersey (1999)
29. Lusi, M.: A rough guide to molecular solid solutions: design, synthesis and characterization of mixed crystals. CrystEngComm **20**, 7042–7052 (2018)
30. Bastos, T.S., Rodriguez Reartes, S.B., Zabaloy, M.S., Cassaro, R.F., Bazito, R.C., Borges, G.R., Dariva, C., Franceschi, E.: Phase behavior for the system carbon dioxide + *p*-nitrobenzaldehyde: experimental and modeling. J. Chem. Eng. Data **64**, 2116–2125 (2019)
31. Porras Giraldo, A.F., Rodriguez-Reartes, S.B., Zabaloy, M.S.: A solid solution modeling approach somehow analogous to the Eos approach for fluids: application to equilibria involving fluid phases and solid solutions. Fluid Phase Equilib. **547**, 113174 (2021)
32. Michelsen, M.L., Mollerup, J.M.: Thermodynamic Models: Fundamentals and Computational Aspects. Tie-Line Publications (2004)
33. Aiche: DIPPR 801, Design Institute for Physical Property Data Public Release Evaluated Process Design Data, BYU-DIPPR, Thermoph, (2003)
34. Hukkerikar, A.S., Sarup, B., Ten Kate, A., Abildskov, J., Sin, G., Gani, R.: Group-contribution + (GC +) based estimation of properties of pure components: improved property estimation and uncertainty analysis. Fluid Phase Equilib. **321**, 25–43 (2012)

35. Soto, R., Svärd, M., Verma, V., Padrela, L., Ryan, K., Rasmuson, Å.C.: Solubility and thermodynamic analysis of ketoprofen in organic solvents. Int J Pharm (2020). https://doi.org/10.1016/j.ijpharm.2020.119686
36. Espitalier, F., Biscans, B., Peyrigain, P.S., Laguerie, C.: Ternary diagram alpha-(3-benzoylphenyl)-propionic acid (ketoprofen) in acetone-water mixtures at different temperatures. experimental data and predicted results. Fluid Phase Equilib **113**, 151–171 (1995)
37. Wassvik, C.M., Holmén, A.G., Bergström, C.A.S., Zamora, I., Artursson, P.: Contribution of solid-state properties to the aqueous solubility of drugs. Eur. J. Pharm. Sci. **29**, 294–305 (2006)
38. Kommuru, T.R., Khan, M.A., Reddy, I.K.: Racemate and enantiomers of ketoprofen: phase diagram, thermodynamic studies, skin permeability, and use of chiral permeation enhancers. J. Pharm. Sci. **87**, 833–840 (1998)
39. Span, R., Wagner, W.: A new equation of state for carbon dioxide covering the fluid region from the triple-point temperature to 1100 K at pressures up to 800 Mpa. J. Phys. Chem. Ref. Data **25**, 1509–1596 (1996)
40. Chang, H., Morrell, D.G.: Solubilities of methoxy-1-tetralone and methyl nitrobenzoate isomers and their mixtures in supercritical carbon dioxide. J. Chem. Eng. Data **30**, 74–78 (1985)
41. Chen, J.-W., Tsai, F.-N.: Solubilities of methoxybenzoic acid isomers in supercritical carbon dioxide. Fluid Phase Equilib. **107**, 189–200 (1995)
42. Lamb, D.M., Barbara, T.M., Jonas, J.: NM Study of solid naphthalene soiubllities in supercritical carbon dioxide near the upper critical end polnt. J. Phys. Chem. **90**, 4210–4215 (1987)
43. Favareto, R., Pereira, J.R.D., Santana, C.C., Madureira, E.H., Cabral, V.F., Tavares, F.W., Cardozo-Filho, L.: High-pressure phase diagram of the drug mitotane in compressed and/or supercritical CO_2. J. Chem. Thermodyn. **42**, 286–290 (2010)
44. Kurnik, R.T., Holla, S.J., Reid, R.C.: Solubility of solids in supercritical carbon dioxide and ethylene. J. Chem. Eng. Data **26**, 47–51 (1981)
45. McHugh, M., Paulaitis, M.E.: Solid solubilities of naphthalene and biphenyl in supercritical carbon dioxide. J. Chem. Eng. Data **25**, 326–329 (1980)
46. Mitra, S., Chen, J.W., Viswanath, D.S.: Solubility and partial molar volumes of heavy aromatic hydrocarbons in supercritical COP. J. Chem. Eng. Data **33**, 35–37 (1988)
47. Sako, T., Yamane, S., Negishi, A., Sato, M.: Solubility measurement in crossover region of supercritical CO_2–naphthalene–phenanthrene system. J. Jpn. Pet. Inst. **37**, 321–327 (1993)
48. Zúñiga-Moreno, A., Galicia-Luna, L.A., Camacho-Camacho, L.E.: Measurements of solid solubilities and volumetric properties of naphthalene + carbon dioxide mixtures with a new assembly taking advantage of a vibrating tube densitometer. Fluid Phase Equilib. **234**, 151–163 (2005)
49. Jennings, D.W., Lee, R.-J., Teja, A.S.: Vapor–liquid equilibria in the carbon dioxide + ethanol and carbon dioxide + 1-butanol systems. J. Chem. Eng. Data **36**, 167 (1991)
50. Suzuki, K., Sue, H., Itou, M., Smith, R.L., Inomata, H., Arai, K., Saito, S.: Isothermal vapor–liquid equilibrium data for binary systems at high pressures: carbon dioxide–methanol, carbon dioxide–ethanol, carbon dioxide–*i*-propanol, methane–ethanol, methane–*i*-propanol, ethane–ethanol, and ethane–*i*-propanol systems. J. Chem. Eng. Data **35**, 63–66 (1990)
51. Knez, Ž, Škerget, M., Ilič, L., Lütge, C.: Vapor–liquid equilibrium of binary CO_2–organic solvent systems (ethanol, tetrahydrofuran, ortho-xylene, meta-xylene, para-xylene). J. Supercrit. Fluids **43**, 383–389 (2008)
52. Weinstein, R.D., Muske, K.R., Moriarty, J., Schmidt, E.K.: The Solubility of benzocaine, lidocaine, and procaine in liquid and supercritical carbon dioxide. J. Chem. Eng. Data **49**, 547–552 (2004)
53. Wubbolts, F.E., Bruinsma, O.S.L., Van Rosmalen, G.M.: Measurement and modelling of the solubility of solids in mixtures of common solvents and compressed gases. J. Supercrit. Fluids **32**, 79–87 (2004)

Authors and Affiliations

José Vinicius Mattos[1] · Matías José Molina[2,3] · Sabrina Belén Rodriguez-Reartes[2,3,5] · Leandro Ferreira-Pinto[4] · Marcelo Santiago Zabaloy[2,3] · Lúcio Cardozo-Filho[1]

✉ Lúcio Cardozo-Filho
lcfilho@uem.br

[1] Departamento de Engenharia Química, Universidade Estadual de Maringá (UEM), Av. Colombo 5790, Maringá, Brasil

[2] Planta Piloto de Ingeniería Química-PLAPIQUI (UNS-CONICET), Camino "La Carrindanga" Km 7, 8000 Bahía Blanca, Argentina

[3] Departamento de Ingeniería Química, Universidad Nacional del Sur (UNS), Avda. Alem 1253, Bahía Blanca, Argentina

[4] Departamento de Engenharia de Energia, Universidade Estadual Paulista (UNESP), Av. Dos Barrageiros 1881, Primavera, Rosana, Brasil

[5] Department of Chemical Engineering (ETSEQ), Universitat Rovira i Virgili, Avinguda Països Catalans 26, 43007, Tarragona, Spain